

## CCD PHOTOMETRY AND EVOLUTIONARY STATUS OF THE HADS VARIABLE PT COM

K. B. Alton

Desert Blooms Observatory, USA.

Received October 26 2021; accepted February 10 2022

### ABSTRACT

Multi-color ( $BVI_c$ ) CCD-derived photometric data were acquired from PT Com, a pulsating variable classified as a high amplitude  $\delta$  Scuti-type system. Analysis of precise time-series lightcurve data was accomplished using discrete Fourier transformation which revealed a mean fundamental mode ( $f_0$ ) of oscillation at  $12.178364 \pm 0.000083 \text{ d}^{-1}$  along with at least three other partial harmonics ( $2f_0$ ,  $3f_0$  and  $4f_0$ ). No other statistically significant frequency shared by all bandpasses was resolved following successive pre-whitening of each residual signal. A secular analysis of the fundamental pulse period since 1999 was facilitated by the addition of 35 new times-of-maximum. The evolutionary status, age and physical nature of PT Com were investigated using the PAdova & TRieste Stellar Evolution Code for generating stellar tracks and isochrones.

### RESUMEN

Mediante fotometría CCD se obtuvieron datos multicolores ( $BVI_c$ ) para PT Com, una variable pulsante clasificada como un sistema tipo  $\delta$  Scuti de gran amplitud. El análisis de los datos precisos para la curva de luz se efectuó usando la transformación discreta de Fourier, la cual reveló un modo fundamental medio de oscilación ( $f_0$ ) en  $12.178364 \pm 0.000083 \text{ d}^{-1}$ , además de por lo menos tres armónicos parciales ( $2f_0$ ,  $3f_0$  y  $4f_0$ ). No se encontró otra frecuencia estadísticamente significativa compartida por todos los anchos de banda, después del pre-blanqueado de cada señal residual. El análisis secular del período fundamental a partir de 1999 se facilitó con la adición de 35 nuevos tiempos de máximo. Se investigó el estado evolutivo, la edad y la naturaleza física de PT Com usando el código de evolución estelar PAdova & TRieste para generar trayectorias evolutivas e isocronas.

*Key Words:* stars: evolution — stars: oscillations — stars: variables: Delta Scuti

### 1. INTRODUCTION

High amplitude  $\delta$  Scuti stars, hereafter HADS, represent a very small percentage (<1%) of all  $\delta$  Sct variables (Lee et al. 2008). Driven by the  $\kappa$ -mechanism (opacity pump) resulting from partial ionization of He II (Pamyatnykh 1999), they commonly oscillate ( $\Delta V > 0.1 \text{ mag}$ ) via low-order single or double radial pulsation modes (Poretti 2003a,b; Niu et al. 2013, 2017). Many ( $\approx 40\%$ ) are double pulsators exhibiting simultaneous pulsations in the fundamental and the first overtone mode with amplitudes generally higher in the fundamental mode (McNamara 2000). Although uncommon, non-radial pulsations were detected in the HADS variable V974 Oph

(Poretti 2003a,b). HADS variables have historically been divided according to metallicity relative to the Sun where  $[\text{Fe}/\text{H}]$  is defined as zero. The metal-poor ( $[\text{Fe}/\text{H}] \ll 0$ ) group is classified as SX Phe-like stars based on the prototype SX Phoenicis. Ostensibly they have shorter periods ( $0.02 < P < 0.125 \text{ d}$ ) and lower masses ( $\approx 1.0\text{--}1.3 M_\odot$ ) than their related HADS variables possessing near solar metal abundance (McNamara 2011). SX Phe stars frequently reside in globular clusters (GC) which are ancient collections of Population II stars. The majority of these pulsators are classified as blue straggler stars, paradoxically appearing much younger than their GC cohorts. Balona & Nemeč (2012) proposed that

it is not possible to differentiate between  $\delta$  Sct and field SX Phe variables based on pulsation amplitude, the number of pulsation modes, period or even metallicity (Garg et al. 2010). Much more sensitive space instruments like NASA’s Kepler (Gilliland et al. 2010; Guzik 2021), the European Space Agency’s CoRoT (Baglin 2003) and the Canadian’s Microvariability and Oscillations of STars [MOST] (Walker et al. 2003) have found many examples that violate the traditional differentiation between HADS and SX Phe pulsators. Balona & Nemeč (2012) further contend that the evolutionary status of each star is the only way to distinguish between these two classes.

An additional classification scheme for  $\delta$  Scuti stars was recently proposed by Qian et al. (2018) wherein two distinct groups of  $\delta$  Scuti stars were uncovered from the LAMOST survey that fundamentally differed in effective temperature. One group was identified as normal  $\delta$  Scuti stars (NDSTs) when  $T_{\text{eff}}$  ranged between 6700–8500 K while the other defined as unusual and cool variable stars (UCVs) with  $T_{\text{eff}}$  had values less than 6700 K. A more restrictive fundamental pulsation range (0.09–0.22 d) coupled with being slightly metal poor ( $[\text{Fe}/\text{H}] = -0.25 - 0.0$ ) further differentiates the UCVs from the NDST group. Furthermore, once the UCV stars were excluded from consideration, empirically based temperature-period, log g-period, and metallicity-period relationships were derived for NDSTs like PT Com.

The variability of PT Com (J2000–12:13:40.7640 +17h 14m 37.84;  $l = 259.5536$   $b = 76.8169$ ) was first recorded in unfiltered photometric data collected during the ROTSE-I Survey (Akerlof et al. 2000; Woźniak et al. 2004). Additional monochromatic CCD-derived lightcurve data were captured from the Catalina Sky Survey<sup>1</sup> (Drake et al. 2009), the All Sky Automated Survey<sup>2</sup> (Pojmanski 2000), the All Sky Automated Survey for Supernovae<sup>3</sup> (Shappee et al. 2014). Other photometric data which ultimately lead to the determination of time-to-maximum (ToMx) light values were reported by Wunder (2012) and Wils et al. (2014). This report marks the first multi-bandpass photometric study on PT Com which also provides a detailed Fourier analysis of this radial pulsator and critically assesses its classification as a HADS variable.

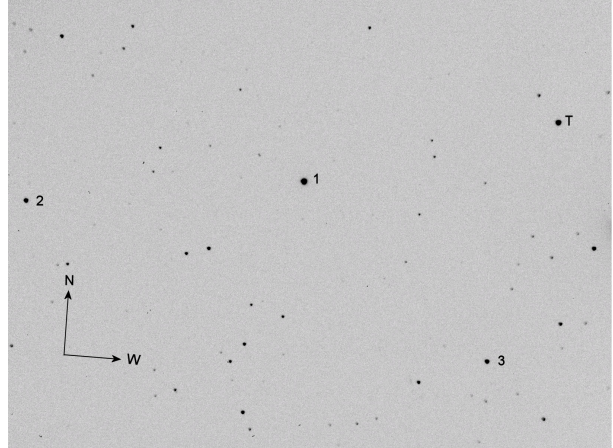


Fig. 1. FOV (15.9×21.1 arcmin) containing PT Com (T) along with the three comparison stars (1-3) used to reduce time-series images to APASS-catalog based magnitudes.

## 2. OBSERVATIONS AND DATA REDUCTION

Precise time-series images were acquired at Desert Blooms Observatory (DBO, USA – 31.941 N, 110.257 W) using a QSI 683 wsg-8 CCD camera mounted at the Cassegrain focus of a 0.4-m Schmidt-Cassegrain telescope. A Taurus 400 (Software Bisque) equatorial fork mount facilitated continuous operation without the need to perform a meridian flip. The image (science, darks, and flats) acquisition software (TheSkyX Pro Edition 10.5.0) controlled the main and integrated guide cameras. This focal-reduced ( $f/7.2$ ) instrument produces an image scale of 0.76 arcsec/pixel (bin=2×2) and a field-of-view (FOV) of 15.9×21.1 arcmin. The CCD camera is equipped with  $B$ ,  $V$  and  $I_c$  filters manufactured to match the Johnson-Cousins Bessell prescription. Dark subtraction, flat correction and registration of all images collected at DBO were performed using *AIP4Win* v2.4.0 (Berry & Burnell 2005). Instrumental readings were reduced to catalog-based magnitudes using the AAVSO Photometric All-Sky Survey (APASS) star fields (Henden et al. 2009, 2010, 2011; Smith et al. 2011) built into *MPO Canopus* v10.7.1.3 (Minor Planet Observer). An image showing the FOV for PT Com (T) and the ensemble of three non-varying comparison stars (1-3) is shown in Figure 1. The identity (HST Guide Star Catalog, Version GSC-ACT), Gaia DR2 J2000 coordinates and APASS color indices ( $B-V$ ) for these stars are provided in Table 1. Since all program stars share a relatively small FOV, differential atmospheric extinction was ignored while data from images taken below 30° altitude (airmass >2.0) were excluded.

<sup>1</sup><http://nesssi.cacr.caltech.edu/DataRelease/>.

<sup>2</sup><http://www.astrouw.edu.pl/asas/?page=acvs>.

<sup>3</sup><https://asas-sn.osu.edu/variables>.

TABLE 1  
GAIA DR2 ASTROMETRIC COORDINATES (J2000)\*

FOV ID	GSC ID	R.A. h m s	Dec. deg m s	APASS <sup>a</sup> V-mag	APASS <sup>a</sup> (B-V)
T	1442-01358	12 13 40.7799	+17 14 37.811	11.982	0.279
1	1442-02386	12 14 19.7713	+17 11 46.075	10.754	0.791
2	1442-00715	12 13 49.2064	+17 05 34.357	13.375	0.410
3	1442-00175	12 15 02.7262	+17 10 18.301	13.073	0.708

\*V-mag and color indices (B-V) for PT Com (GSC 1442-01358) and three comparison stars (1-3).

<sup>a</sup>V-mag and (B-V) derived from APASS DR9 database.

### 3. RESULTS

Photometric values in  $B$  ( $n=304$ ),  $V$  ( $n=305$ ), and  $I_c$  ( $n=301$ ) passbands were each processed to produce LCs that encompassed 25Mar2019 through 09April2019 (Figure 2). Times-of-maximum (ToMx) and associated errors were calculated according to Andrych & Andronov (2019) and Andrych et al. (2020) using the program MAVKA (<https://uavso.org.ua/mavka/>). Simulation of extrema was automatically optimized by finding the most precise degree ( $\alpha$ ) and best fit algebraic polynomial expression. This procedure, along with eight additional methods featured in MAVKA, are also well suited for other variable star LCs with symmetric or asymmetric extrema. Fundamental pulsation timing differences (PTD) *vs.* epoch were fit using scaled Levenberg-Marquardt algorithms (*QtiPlot* 0.9.9 – rc9; <https://www.qtiplot.com/>). Photometric uncertainty was calculated according to the so-called “CCD Equation” (Mortara & Fowler 1981; Howell 2006). During each imaging session brightness uncertainty typically stayed within  $\pm 0.006$  mag for all three passbands. All relevant lightcurve data (HJD, APASS magnitude, err, filter) acquired during this study at DBO can be retrieved from the AAVSO archives (<https://www.aavso.org/data-download>). The sum total of all ToMx values included 30 from the literature (Wunder 2012; Wils et al. 2014), 12 acquired at DBO, 5 determined from V-mag LCs archived at the British Astronomical Association (BAA) website (<https://britastro.org/photdb/data.php>) and 18 derived from V-mag light curve data downloaded from the AAVSO VSX archives (<https://www.aavso.org/data-download>). These results, which appear in Table 2, were used to evaluate possible changes in the fundamental pulse period. In this case, the relationship between PTD and cycle number can be described by a straight line relationship (Figure 3) from

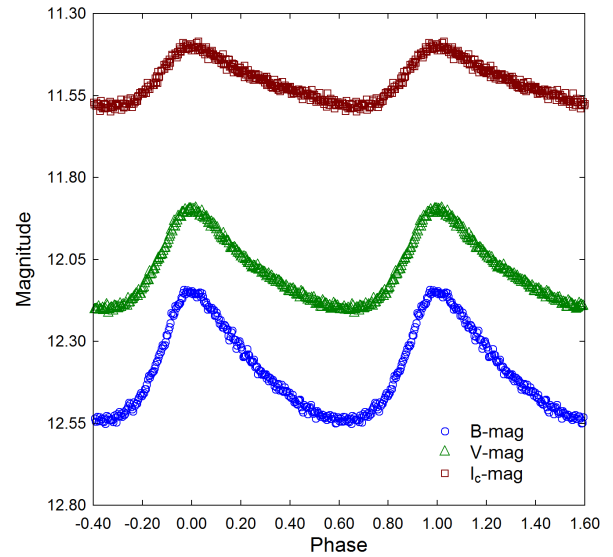


Fig. 2. Period folded ( $0.082112 \pm 0.000001$  d) LCs for PT Com produced from photometric data obtained between 25Mar2019 and 09April2019 at DBO. LCs shown at the top ( $I_c$ ), middle (V) and bottom (B) represent catalog-based (APASS) magnitudes determined using *MPO Canopus*. The color figure can be viewed online.

which a new linear ephemeris was calculated (equation 1):

$$Max(HJD) = 2\,459\,291.4777(4) + 0.082112(1) E. \quad (1)$$

These results suggest that fundamental pulsation period has probably not changed since 1999. Furthermore period folded LCs from ASAS-SN photometric data acquired between 2013 and 2018 were very closely matched to V-mag LCs observed in 2019 at DBO (Figure 4). This would suggest the pulsation amplitude has also remained constant since at least 2013.

TABLE 2  
PT COM: ToMx, MEASUREMENT UNCERTAINTY, EPOCH, PTD\*

ToMx (HJD-2400000)	Err	Cycle No.	PTD.	Ref.	ToMx (HJD-2400000)	Err	Cycle No.	PTD.	Ref.
51315.9736	nr	-97129	-0.0004	1	58173.4359	0.0003	-13616	0.0018	4
51543.9968	nr	-94352	-0.0036	1	58173.5152	0.0001	-13615	-0.0010	4
51617.9821	nr	-93451	-0.0016	1	58174.4189	0.0007	-13604	-0.0005	4
52638.0710	nr	-81028	0.0039	1	58174.5014	0.0005	-13603	-0.0002	4
53740.0178	nr	-67608	0.0011	1	58176.4722	0.0006	-13579	-0.0001	4
54204.8604	nr	-61947	0.0049	1	58176.5539	0.0009	-13578	-0.0005	4
54867.8317	nr	-53873	-0.0001	1	58177.4557	0.0010	-13567	-0.0019	4
54878.0105	nr	-53749	-0.0032	1	58177.5410	0.0003	-13566	0.0013	4
54886.8852	nr	-53641	0.0034	1	58197.4102	0.0005	-13324	-0.0007	4
55185.0275	nr	-50010	-0.0047	1	58197.4928	0.0010	-13323	-0.0003	4
55209.0082	nr	-49718	-0.0009	1	58204.3900	0.0005	-13239	-0.0005	4
55268.8637	nr	-48989	-0.0054	1	58204.4717	0.0006	-13238	-0.0009	4
55276.8340	nr	-48892	0.0001	1	58462.7156	0.0006	-10093	-0.0008	4
55290.7106	nr	-48723	-0.0004	1	58528.4882	0.0011	-9292	-0.0003	4
55336.6942	nr	-48163	0.0002	1	58529.6386	0.0003	-9278	0.0006	3
55358.7005	nr	-47895	0.0004	1	58529.7222	0.0004	-9277	0.0020	3
55576.9530	nr	-45237	-0.0021	1	58532.5111	0.0001	-9243	-0.0009	4
55615.9575	nr	-44762	-0.0011	1	58567.7378	0.0001	-8814	-0.0005	5
55681.8179	nr	-43960	0.0051	1	58567.8195	0.0003	-8813	-0.0008	5
55959.8484	nr	-40574	0.0027	1	58567.9022	0.0002	-8812	-0.0003	5
55975.9468	nr	-40378	0.0071	1	58571.6788	0.0001	-8766	-0.0008	5
55988.8347	nr	-40221	0.0033	1	58571.7618	0.0001	-8765	0.0001	5
56035.7996	nr	-39649	-0.0001	1	58571.8430	0.0002	-8764	-0.0009	5
56072.4203	nr	-39203	-0.0016	1	58571.9255	0.0002	-8763	-0.0005	5
56073.4062	nr	-39191	-0.0010	1	58573.7323	0.0001	-8741	-0.0002	5
56075.3756	nr	-39167	-0.0023	1	58573.8143	0.0001	-8740	-0.0003	5
56075.4602	nr	-39166	0.0002	1	58573.8969	0.0001	-8739	0.0003	5
56076.4441	nr	-39154	-0.0013	1	58582.7641	0.0002	-8631	-0.0007	5
56354.8875	0.0004	-35763	-0.0013	2	58582.8465	0.0002	-8630	-0.0004	5
56358.8290	0.0006	-35715	-0.0012	2	58587.4455	0.0013	-8574	0.0002	4
56721.6072	0.0003	-31297	0.0040	3	59271.5245	0.0002	-243	0.0001	3
58171.4657	0.0005	-13640	0.0023	4	59291.4786	0.0002	0	0.0007	3
58171.5463	0.0004	-13639	0.0008	4					

\*ToMx: Times of maximum.

PTD: fundamental pulsation timing differences used to calculate a linear ephemeris.

nr=not reported.

1. Wunder (2012); 2 Wils et al. (2014); 3 BAA; 4. AAVSO; 5. This study at DBO.

### 3.1. Light Curve Behavior

Morphologically, LCs from HADS variables are asymmetrical with a rapid increase in brightness producing a sharply defined maximum peak. Thereafter a slower decline in magnitude results in a broad minimum. The largest difference between maximum and minimum light is observed in the blue passband

( $\Delta B = 0.39$  mag), followed by V ( $\Delta V = 0.27$  mag) and finally the smallest difference detected in infrared ( $\Delta I_c = 0.18$  mag). Plotting  $(B-V)_0$  against phase (Figure 5) shows significant color amplitude (0.11 mag) going from maximum [ $(B-V) \simeq 0.20$ ] to minimum light [ $(B-V) \simeq 0.31$ ]. This behavior is commonly observed with pulsating F- to A-type stars.

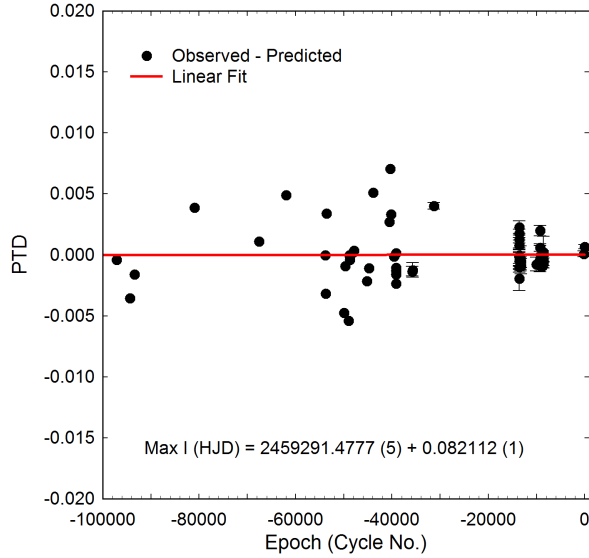


Fig. 3. Straight line fit (PTD vs. cycle number) suggesting that little or no change to the fundamental pulsation period of PT Com had occurred between 1999 and 2021. The color figure can be viewed online.

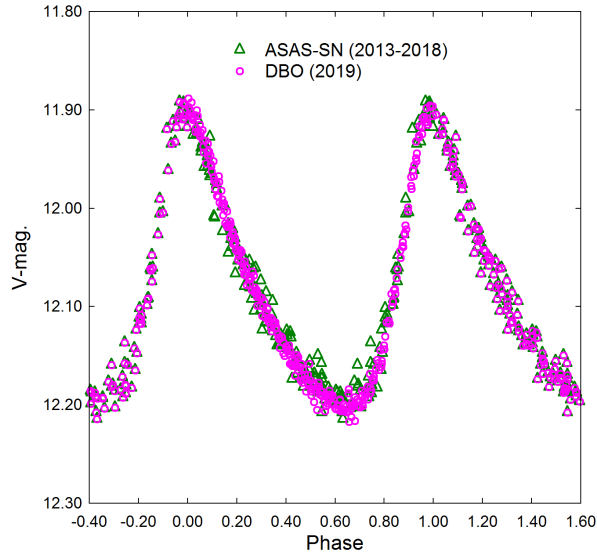


Fig. 4. Period folded ( $0.082113 \pm 0.000008$  d) LCs for PT Com produced from photometric data obtained between 2013 and 2018 (ASAS-SN) and in 2019 at DBO. The color figure can be viewed online.

Interstellar extinction was estimated according to Amôres & Lépine (2005)<sup>5</sup> which requires galactic coordinates ( $l$ ,  $b$ ) and distance (kpc). Accordingly, the Model A reddening value,

<sup>5</sup><http://www.galexin.org/>.

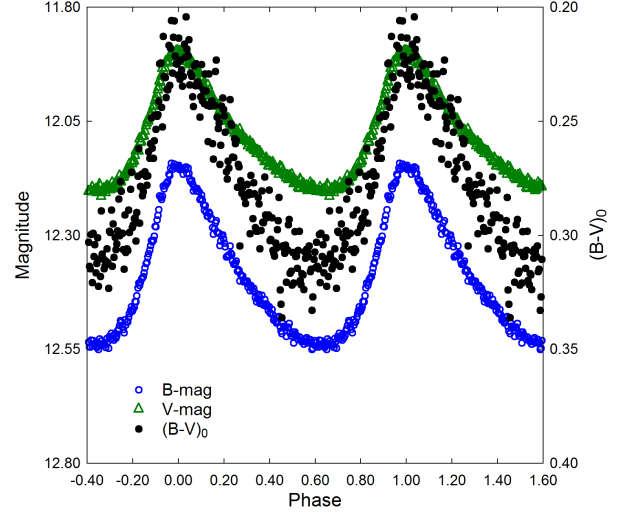


Fig. 5. PT Com LC illustrating significant color change as maximum light [ $(B-V)_0 \simeq 0.20$  mag.] slowly descends to minimum light [ $(B-V)_0 \simeq 0.31$  mag.]. The color figure can be viewed online.

$E(B-V) = 0.0270 \pm 0.0001$  mag, corresponds to an intrinsic color index  $(B-V)_0$  for PT Com that varies between  $0.194 \pm 0.024$  at maximum light and  $0.309 \pm 0.016$  mag at minimum brightness. The average effective temperature ( $T_{\text{eff}}$ ) was estimated to be  $7473 \pm 157$  K according to the polynomial transformation equations derived by Flower (1996). These results based strictly on  $(B-V)$  photometry at DBO are somewhat lower but within the uncertainty included ( $T_{\text{eff}} = 7801^{+470}_{-204}$  K) in the Gaia DR2 release of stellar parameters (Andrae et al. 2018). The final  $T_{\text{eff}}$  ( $7451 \pm 186$  K) adopted for this study represents a median value from 2MASS ( $6953 \pm 245$  K) using  $J$ ,  $K$  and  $H$  transforms (Warner 2007) to Johnson-Cousins, Gaia DR2, LAMOST DR5 ( $7429 \pm 32$ ) and DBO ( $7473 \pm 157$  K). According to Pecaut & Mamajek (2013) the spectral type of this variable would likely range between A7 and A9. A low resolution UV-vis spectrum has been reported by LAMOST DR5 (Zhao et al. 2012; Wang et al. 2019) which is consistent with an A7V classification for PT Com. According to Qian et al. (2018), PT Com would be considered a NDST rather than a UCV since  $T_{\text{eff}}$  is between 6700 and 8500 K while the fundamental pulsation period is less than 0.09 d.

### 3.2. Lightcurve Analysis by Discrete Fourier Transformation

Discrete Fourier transformation (DFT) was used to extract the fundamental pulsating frequency (spectral window = 100 d<sup>-1</sup>) using *Period04* (Lenz & Breger 2005). Pre-whitening steps which successively remove the previous most intense signals were employed to extract other potential oscillations from the residuals. Only those frequencies with a S/N<sub>≥</sub>6 (Baran et al. 2015) in each passband are presented in Table 3. In all cases, uncertainties in frequency, amplitude, and phase were estimated by the Monte Carlo simulation ( $n=400$ ) routine featured in *Period04*. Representative amplitude spectra from *B*-mag data acquired at DBO are shown in Figure 6. Since the oscillation frequencies obtained from *V*- and *I<sub>c</sub>*-bandpasses are essentially redundant, they are not provided herein. A representative DFT-derived model fit with residual error indicates a very good fit for LC (*B*-mag) data acquired on 29Mar2019 (Figure 7). The amplitude decay for PT Com appears to be exponential as a function of harmonic order (Figure 8) a behavior consistent with other HADS variables such as VX Hyd (Templeton et al. 2009), RR Gem (Jurcsik et al. 2005) and V460 And (Alton & Stepień 2019).

### 3.3. Global Parameters

Ever since a period-luminosity relationship (PLR) between 25 Cepheid variables in the Small Magellanic Cloud was discovered (Leavitt & Pickering 1912), pulsating stars have served as standard candles for estimating cosmic distances to individual stars, clusters and galaxies. A new PLR (Ziaali et al. 2019) was adopted herein, which for the most part was established using the thus far most accurate distance values determined from parallax during the Gaia Mission (Lindegren et al. 2016; Luri et al. 2018). Accordingly this empirically-derived expression (equation 2):

$$M_V = (-2.94 \pm 0.06) \log(P) - (1.34 \pm 0.06), \quad (2)$$

is similar to the equation published by McNamara (2011) but with somewhat improved precision.

Absolute  $V_{\text{mag}}$  ( $M_V$ ) was estimated ( $1.85 \pm 0.17$ ) after substituting the fundamental pulsation period (0.082112 d) into equation 2. The reddening corrected distance modulus (equation 3):

$$d(\text{pc}) = 10^{(m - M_V - A_V + 5)/5} \quad (3)$$

produced an estimated distance ( $1062 \pm 83$  pc) to PT Com using observed values for  $m$

( $V_{\text{avg}}=12.065 \pm 0.021$ ) and  $A_V$  ( $0.0836 \pm 0.0003$ ). By comparison, the Gaia DR2 parallax-derived distance (Bailer-Jones 2015) reported for this variable ( $1108^{+92}_{-79}$ ) is just 4% farther.

The pulsation period and temperature/color were measured by direct observation. Similarly, the solar luminosity ( $13.86 \pm 2.15$ ) was determined from equation 4:

$$L_*/L_\odot = 10^{((M_{\text{bol}\odot} - M_{\text{bol}*})/2.5)}, \quad (4)$$

when  $M_{\text{bol}\odot}=4.74$ ,  $M_V=1.85 \pm 0.17$  and  $BC=0.034$  then  $M_{\text{bol}*}=1.89 \pm 0.17$ .

Photometric and spectroscopic observation of eclipsing binary stars are commonly used to determine component mass by applying the laws of gravity derived by Isaac Newton and Johannes Kepler. In contrast, the mass of an isolated field star like PT Com is very difficult to determine by direct measurement. However, it is possible under certain conditions ( $1.05 < M_\odot \leq 2.40$ ) to estimate mass according to Eker et al. (2018), who derived a mass-luminosity relationship from main sequence (MS) stars in detached binary systems. This expression (equation 5):

$$\log(L) = 4.329(\pm 0.087) \cdot \log(M) - 0.010(\pm 0.019), \quad (5)$$

leads to its mass in solar units ( $1.85 \pm 0.07 M_\odot$ ). Fairly typical for a HADS variable, this result and all others derived from DBO data are summarized in Table 4. Finally, the radius in solar units ( $R_* = 2.23 \pm 0.17$ ) was estimated using the well-known relationship (equation 6):

$$L_*/L_\odot = (R_*/R_\odot)^2 (T_*/T_\odot)^4. \quad (6)$$

Derived values for density ( $\rho_\odot$ ), surface gravity ( $\log g$ ), and pulsation constant ( $Q$ ) are also included in Table 4. Stellar density ( $\rho_*$ ) in solar units ( $\text{g}/\text{cm}^3$ ) was calculated according to equation 7:

$$\rho_* = 3 \cdot G \cdot M_* \cdot m_\odot / (4\pi (R_* \cdot r_\odot)^3), \quad (7)$$

where  $G$  is the *cgs* gravitational constant,  $m_\odot$ =solar mass ( $g$ ),  $r_\odot$ =solar radius (cm),  $M_*$  is the mass and  $R_*$  the radius of PT Com in solar units. Using the same algebraic assignments, surface gravity ( $\log g$ ) was determined by the following expression (equation 8):

$$\log g = \log(M_* \cdot m_\odot \cdot G / (R_* \cdot r_\odot)^2). \quad (8)$$

The dynamical time that it takes a p-mode acoustic wave to internally traverse a star is strongly correlated to the stellar mean density. The pulsation

TABLE 3  
 FUNDAMENTAL FREQUENCY ( $d^{-1}$ ) AND CORRESPONDING PARTIAL HARMONICS\*

	Freq. ( $d^{-1}$ )	Freq. Err	Amp. (mag)	Amp. Err	Phase	Phase Err	Amp. S/N
$f_0$ -B	12.1786	0.0001	0.1768	0.0006	0.5225	0.0006	202.5
$f_0$ -V	12.1782	0.0001	0.1349	0.0005	0.6903	0.0006	322.7
$f_0$ -I <sub>c</sub>	12.1770	0.0004	0.0796	0.0010	0.5688	0.0026	81.0
$2f_0$ -B	24.3576	0.0004	0.0519	0.0007	0.4978	0.0021	49.2
$2f_0$ -V	24.3568	0.0004	0.0429	0.0005	0.7744	0.0019	102.1
$2f_0$ -I <sub>c</sub>	24.3572	0.0411	0.0272	0.0062	0.0203	0.0557	33.7
$3f_0$ -B	36.5344	0.0011	0.0194	0.0007	0.4159	0.0056	20.9
$3f_0$ -V	36.5336	0.0814	0.0149	0.0021	0.4487	0.0635	23.1
$3f_0$ -I <sub>c</sub>	36.5374	0.0043	0.0080	0.0009	0.6356	0.0259	9.7
$4f_0$ -B	48.7169	0.0043	0.0067	0.0018	0.7035	0.1571	7.2
$4f_0$ -V	48.7103	0.0036	0.0042	0.0005	0.1210	0.0196	7.2

\*Detected following DFT analysis of time-series photometric data ( $BVI_c$ ) from PT Com.

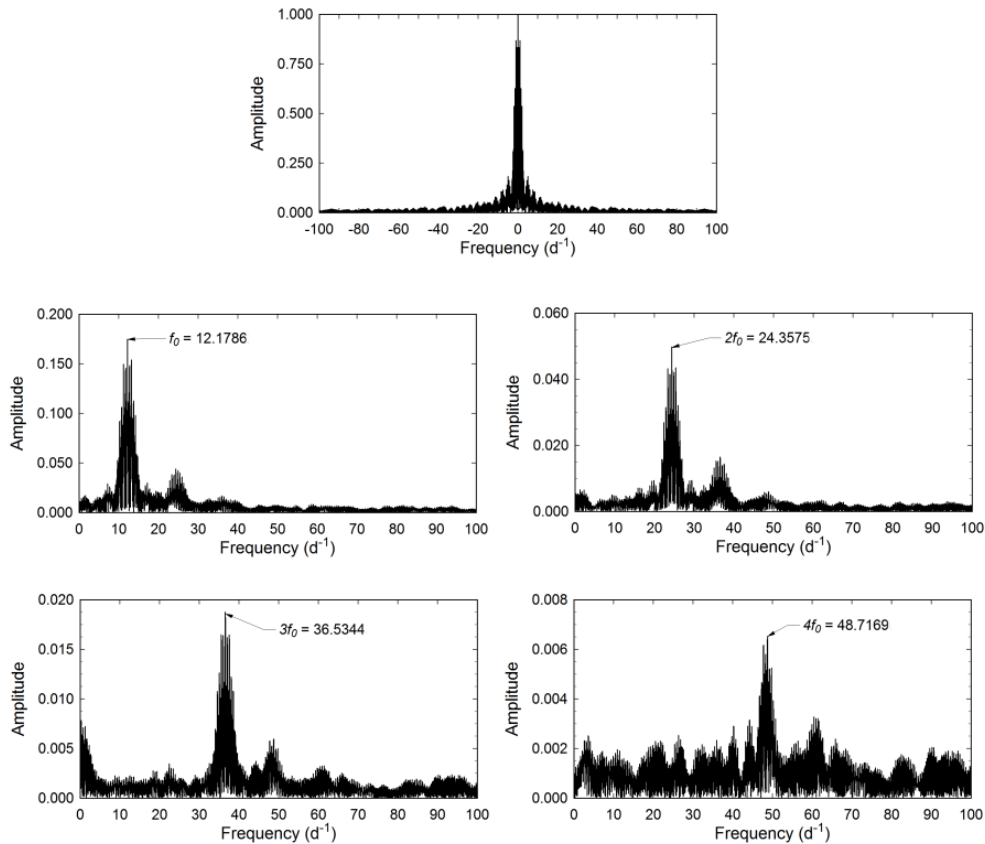


Fig. 6. Spectral window (top panel) and amplitude spectra ( $f_0$ ,  $2f_0$ ,  $3f_0$  and  $4f_0$ ) showing all significant pulsation frequencies following DFT analysis of  $B$ -mag photometric data from PT Com acquired at DBO between 25Mar2019 and 09April2019.

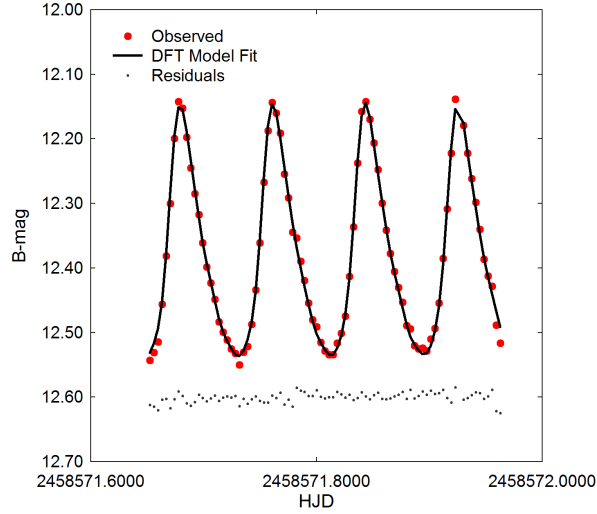


Fig. 7. DFT model fit from LC data ( $B$ -mag) acquired on 29 March 2019 at DBO. Residuals have been offset by a constant amount to compress the  $y$ -axis scale. The color figure can be viewed online.

constant ( $Q$ ) is defined by the period-density relationship (equation 9):

$$Q = P \sqrt{\bar{\rho}_* / \bar{\rho}_\odot}, \quad (9)$$

where  $P$  is the pulsation period (d) and  $\bar{\rho}_*$  and  $\bar{\rho}_\odot$  are the mean densities of the target star and Sun, respectively. The mean density can be expressed (equation 10) in terms of other measurable stellar parameters where:

$$\log(Q) = -6.545 + \log(P) + 0.5 \log(g) + 0.1 M_{bol} + \log(T_{eff}). \quad (10)$$

The full derivation of this expression can be found in Breger (1990). The resulting  $Q$  values provided in Table 4 are within the expected value ( $Q=0.03$ - $0.04$  d) from fundamental radial pulsations observed for other  $\delta$  Sct variables (Breger & Bregman 1975; Breger 1979; Joshi & Joshi et al. 2015; Antonello & Pastori 2005).

Finally, a comparative sense of how the physical size, temperature and brightness of PT Com changes over the duration of a single 1.97 hr pulsation can be estimated. As shown in Figure 4 there is a significant increase in reddening ( $B-V$ ) as maximum light descends to minimum light. Intrinsic color reveals that at maximum light, where  $(B-V)_0 = 0.194 \pm 0.024$ , the corresponding effective temperature is  $7802 \pm 143$  K,

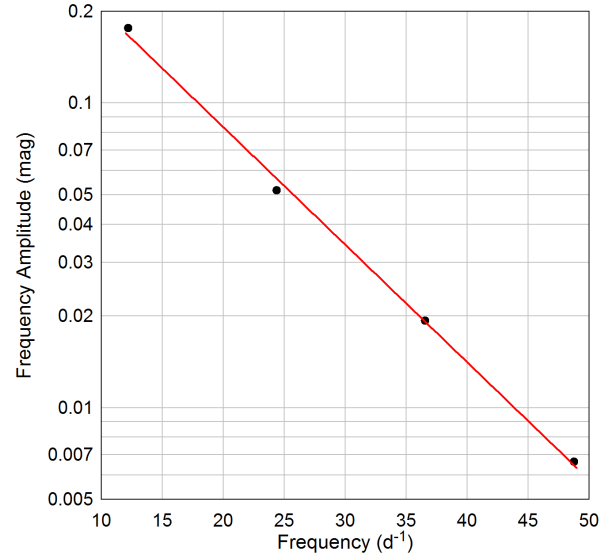


Fig. 8. Log-linear amplitude decay of the fundamental ( $f_0$ ) pulsation period and its corresponding partial harmonics ( $2f_0$ - $4f_0$ ) observed in the  $B$ -passband. The color figure can be viewed online.

TABLE 4

GLOBAL STELLAR PARAMETERS FOR PT COM\*

Parameter	DBO	PARSEC ( $Z=0.020$ )
Mean $T_{\text{eff}}$ [K]	$7451 \pm 186$	$7451 \pm 186$
Luminosity [ $L_\odot$ ]	$13.86 \pm 2.15$	$13.86 \pm 2.15$
Mass [ $M_\odot$ ]	$1.85 \pm 0.07$	$1.79 \pm 0.05$
Radius [ $R_\odot$ ]	$2.23 \pm 0.17$	$2.23 \pm 0.03$
$\rho$ [ $\text{g}/\text{cm}^3$ ]	$0.236 \pm 0.055$	$0.228 \pm 0.011$
$\log g$ [cgs]	$4.011 \pm 0.067$	$3.994 \pm 0.017$
$Q$ [d]	$0.034 \pm 0.003$	$0.033 \pm 0.002$

\*Using values reported from observations at DBO and those predicted from evolutionary modelling.

whereas at minimum light ( $(B-V)_0 = 0.309 \pm 0.016$ ) the estimated effective temperature is  $7170 \pm 84$  K. Between these two extremes the putative rise in temperature (+632 K) would correspond to a 1.3-fold increase in luminosity despite an 8% decrease in surface area ( $\Delta R_\odot = 3.9\%$ ). This inferred estimate for measuring changes in the angular diameter during each pulsation cycle might best be performed with a modern adaptation of the Baade-Wesselink method (Wesselink 1946) using optical interferometers<sup>5</sup>.

<sup>5</sup>[http://homepage.oma.be/marting/MIAPP\\_Groenewegen\\_2014.pdf](http://homepage.oma.be/marting/MIAPP_Groenewegen_2014.pdf).

## 4. EVOLUTIONARY STATUS OF PT COM

The evolutionary status of PT Com was evaluated (Figure 9) using the PAdova & TRIeste Stellar Evolution Code (PARSEC) for stellar tracks and isochrones (Bressan et al. 2012) and then plotted ( $\log T_{\text{eff}}$  vs.  $\log(L/L_{\odot})$ ) in a theoretical Hertzsprung-Russell diagram (HRD). The thick solid maroon-colored line defines the zero-age main sequence (*ZAMS*) position for stars with metallicity  $Z=0.020$ . The two broken lines nearly perpendicular to the *ZAMS* delimit the blue (left) and red (right) edges of the theoretical instability strip for radial low-p modes (Xiong et al. 2016). Also included are the positions of several known HADS and SX Phe-type variables (Balona 2018). The solid black circle indicates the position of PT Com using the DBO derived parameters ( $T_{\text{eff}}$  and  $L_{\odot}$ ) provided in Table 4.

Ironically a single undisputed value for metallicity from the star closest to us remains elusive. Over the last few decades, the reference metallicity values used by several authors for computing stellar models have ranged between  $Z=0.012$  and  $0.020$  (Amard et al. 2019). Serenelli et al. (2016) took great exception to a high solar metallicity value ( $Z=0.0196\pm 0.0014$ ) based on *in situ* measurements of the solar wind (von Steiger & Zurbuchen 2016; Vagnozzi et al. 2017) rather than abundance traditionally determined by spectroscopic analysis. Despite the uncertainty in defining an absolute value for  $Z_{\odot}$ , an estimate for metal abundance is still required in order to determine the mass, radius and age of PT Com from theoretical evolutionary tracks. A  $Z$ -value can be estimated indirectly from its Galactic coordinates. According to the following expression (equation 11):

$$z = d \cdot \sin(b), \quad (11)$$

the distance below or above the Galactic plane can be calculated where  $d$  is distance in pc (1108) and  $b$  is the Galactic latitude ( $76.8169^{\circ}$ ) of PT Com. In this case its position  $\approx 1078$  pc above the Galactic plane suggests residence in the thick disc (Li & Zhao 2017) rather than the halo where many metal poor ( $[\text{Fe}/\text{H}] < -1.6$ ) stars like SX Phe-type variables reside (Carollo et al. 2010). Furthermore, Qian et al. (2018) reports an empirical relationship between metallicity ( $[\text{Fe}/\text{H}]$ ) and the fundamental pulsation period  $P$  for an NDST star according to the following (equation 12):

$$[\text{Fe}/\text{H}] = -0.121(\pm 0.026) + 0.92(\pm 0.25) \times P. \quad (12)$$

As expected for a thick disk resident, the predicted value ( $[\text{Fe}/\text{H}] = -0.045 \pm 0.033$ ) suggests that PT Com

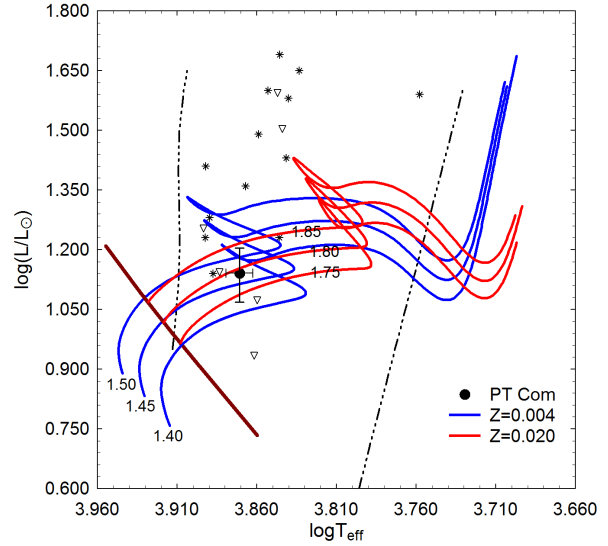


Fig. 9. Evolutionary tracks (red lines;  $Z=0.020$  and blue lines;  $Z=0.004$ ) derived from PARSEC models (Bressan et al. 2012) showing the position of PT Com (black filled circle) relative to *ZAMS* (thick maroon line) and within the theoretical instability strip (black dashed lines) for low-order radial mode  $\delta$  Scuti pulsators. The positions of other HADS (\*) and SX Phe (open triangle) variables reported by Balona (2018) are included for comparison. The color figure can be viewed online.

approaches solar metallicity, or at most a few times lower.

Two separate PARSEC evolutionary models (Bressan et al. 2012) ranging in age between  $1 \times 10^8$  and  $2.21 \times 10^9$  y are illustrated in Figure 9. The red solid lines show the model tracks ( $M_{\odot}=1.75, 1.80$  and  $1.85$ ) over time when  $Z = 0.020$  while the solid blue lines define the metal-poor models ( $M_{\odot}=1.40, 1.45$  and  $1.50$ ) where  $Z = 0.004$ . The latter simulations correspond to a decrease in metallicity by a factor of 3 to 5 depending on the reference solar metallicity. Assuming  $Z = 0.020$ , it can be shown by linear extrapolation that PT Com would have a mass of  $1.79 \pm 0.05 M_{\odot}$  and a radius of  $2.23 \pm 0.03 R_{\odot}$ . The position of this intrinsic variable near the  $M_{\odot}=1.80$  evolutionary track extrapolates to an age of  $1.04 \pm 0.002$  Gyr suggesting it is a moderately evolved MS object lying amongst other HADS variables closer to the blue edge of the instability strip.

By comparison, if PT Com is more metal deficient ( $Z=0.004$ ), then it would have a somewhat greater radius ( $2.61 \pm 0.07 R_{\odot}$ ), but would be less massive ( $1.47 M_{\odot}$ ). Its position closest to the  $1.45 M_{\odot}$  track lies prior to the HRD region where

evolutionary tracks of low metallicity stars begin stellar contraction near the end of core hydrogen burning. This star would still be a MS object but with an age approaching  $2.13 \pm 01$  Gyr. It should be noted that the theoretical mass ( $1.79 M_{\odot}$ ) where  $Z=0.020$  favors the higher metallicity of PT Com is also in good agreement with results ( $1.85 \pm 0.07 M_{\odot}$ ) independently determined using an empirical mass-luminosity relationship. If or when high resolution spectroscopic data become available in the future, uncertainty about the mass and metallicity of PT Com will likely improve.

## 5. CONCLUSIONS

This first multi-bandpass ( $BVI_c$ ) CCD study of PT Com has produced 35 new times-of-maximum. Secular analysis of the ToMx residuals suggests that the fundamental pulsation period has not changed since 1999. Deconvolution of time-series photometric data by discrete Fourier transformation shows that this star is a monoperoiodic radial pulsator ( $f_0=12.1783$  d $^{-1}$ ) which also oscillates in at least 3 other partial harmonics ( $2f_0$ ,  $3f_0$  and  $4f_0$ ). It is conceivable that a more expansive dataset collected at multiple sites over a much longer period of time could reveal other oscillation modes that were not detected in this study. A mean effective temperature for PT Com ( $7451 \pm 186$  K) was estimated from a composite of Gaia DR2, 2MASS, LAMOST DR5 and DBO results, which likely corresponds to spectral type A7-A8. The pulsation period ( $\approx 0.082112$  d), radial oscillation mode,  $V_{\text{mag}}$  amplitude (0.30 mag), spectral type and LC morphology are all consistent with the traditionally defined characteristics of a HADS variable. It should be noted that these attributes do not necessarily exclude the possibility that PT Com is a field SX Phe-type variable. However, the generally accepted threshold for SX Phe stars is  $< 1.3 M_{\odot}$  (McNamara 2011) which in this case is far less than the mass predicted from a  $M-L$  relationship ( $\approx 1.85 M_{\odot}$ ) and evolutionary modeling ( $1.79 \pm 0.05 M_{\odot}$ ). Given these results, the weight of evidence confirms the classification of PT Com as a HADS variable.

This research has made use of the SIMBAD database operated at Centre de Données astronomiques de Strasbourg, France. In addition, the International Variable Star Index maintained by the AAVSO, the Northern Sky Variability Survey hosted by the Los Alamos National Laboratory, the All Sky Automated Survey Catalogue of Variable Stars, the All Sky Automated Survey for Supernovae, and

the Catalina Surveys Data Release 2 archives were mined for essential information. The BAA Photometry Database is acknowledged as partly the source of data on which this article was based. This work also presents results from the European Space Agency (ESA) space mission Gaia. Gaia data are being processed by the Gaia Data Processing and Analysis Consortium (DPAC). Funding for the DPAC is provided by national institutions, in particular those participating in the Gaia MultiLateral Agreement (MLA). The Gaia mission website is <https://www.cosmos.esa.int/gaia> while the Gaia archive website is <https://archives.esac.esa.int/gaia>. The use of public data from LAMOST is also acknowledged. Guoshoujing Telescope (the Large Sky Area Multi-Object Fiber Spectroscopic Telescope LAMOST) is a National Major Scientific Project built by the Chinese Academy of Sciences. Funding for the project has been provided by the National Development and Reform Commission. LAMOST is operated and managed by the National Astronomical Observatories, Chinese Academy of Sciences. The diligence and dedication shown by all associated with these organizations is very much appreciated. The careful review and helpful commentary provided by an anonymous referee is gratefully acknowledged.

## REFERENCES

- Akerlof, C., Amrose, S., Balsano, R., et al. 2000, AJ, 119, 1901, <https://doi.org/10.1086/301321>
- Alton, K. B. & Stepień, K. 2019, AcA, 69, 283, <https://doi.org/10.32023/0001-5237/69.3.4>
- Amard, L., Palacios, A., Charbonnel, C., et al. 2019, A&A, 631, 77, <https://doi.org/10.1051/0004-6361/201935160>
- Amôres, E. B. & Lépine, J. R. D. 2005, AJ, 130, 659, <https://doi.org/10.1086/430957>
- Andrae, R., Fouesneau, M., Creevey, O., et al. 2018, A&A, 616, 8, <https://doi.org/10.1051/0004-6361/201732516>
- Andrych, K. D. & Andronov, I. L. 2019, OEJV, 197, 65, arXiv:1812.06949
- Andrych, K. D., Andronov, I. L., & Chinarova, L. L. 2020, JPhSt, 24, 1902, <https://doi.org/10.30970/jps.24.1902>
- Antonello, E. & Pastori, L. 1981, PASP, 93, 237, <https://doi.org/10.1086/130812>
- Baglin, A. 2003, AdSpR, 31, 345, [https://doi.org/10.1016/S0273-1177\(02\)00624-5](https://doi.org/10.1016/S0273-1177(02)00624-5)
- Bailer-Jones, C. A. L. 2015, PASP, 127, 994, <https://doi.org/10.1086/683116>
- Balona, L. A. & Nemeč, J. M. 2012, MNRAS, 426, 2413, <https://doi.org/10.1111/j.1365-2966.2012.21957.x>
- Balona, L. A. 2018, MNRAS, 479, 183, <https://doi.org/10.1093/mnras/sty1511>

- Baran, A. S., Koen, C., & Porkrzywka, B. 2015, *MNRAS*, 448, 16, <https://doi.org/10.1093/mnras/slu194>
- Berry, R. & Burnell, J. 2005, *The Handbook of Astronomical Image Processing*, (Richmond, VA: Wilmann-Bell)
- Breger, M. 1979, *PASP*, 91, 5, <https://doi.org/10.1086/130433>
- \_\_\_\_\_. 1990, *DSSN*, 2, 13
- Breger, M. & Bregman, J. N. 1975, *ApJ*, 200, 343, <https://doi.org/10.1086/153794>
- Bressan, A., Marigo, P., Girardi, L., et al. 2012, *MNRAS*, 427, 127, <https://doi.org/10.1111/j.1365-2966.2012.21948.x>
- Carollo, D., Beers, T. C., Chiba, M., et al. 2010, *ApJ*, 712, 692, <https://doi.org/10.1088/0004-637X/712/1/692>
- Drake, A. J., Djorgovski, S. G., Mahabal, A., et al. 2009, *ApJ*, 696, 870, <https://doi.org/10.1088/0004-637X/696/1/870>
- Dworak, T. Z. & Zieba, S. 1975, *IBVS*, 1005, 1
- Eker, Z., Bakış, V., Bilir, S., et al. 2018, *MNRAS*, 479, 5491, <https://doi.org/10.1093/mnras/sty1834>
- Flower, P. J. 1996, *ApJ*, 469, 355, <https://doi.org/10.1086/177785>
- Garg, A., Cook, K. H., Nikolaev, S., et al. et al. 2010, *AJ*, 140, 328, <https://doi.org/10.1088/0004-6256/140/2/328>
- Gilliland, R. L., Brown, T. M., Christensen-Dalsgaard, J., et al. 2010, *PASP*, 122, 131, <https://doi.org/10.1086/650399>
- Guzik, J. A. 2021, *FrASS*, 8, 55, <https://doi.org/10.3389/frspas.2021.653558>
- Henden, A. A., Welch, D. L., Terrell, D., & Levine, S. E. 2009, *AAS*, 41, 669
- Henden, A. A., Terrell, D., Welch, D. L., & Smith, T. C. 2010, *AAS*, 42, 515
- Henden, A. A., Levine, S. E., Terrell, D., Smith, T. C., & Welch, D. L. 2011, *AAS*, 43, 2011
- Howell, S. B. 2006, *Handbook of CCD Astronomy* (Cambridge, UK: CUP)
- Joshi, S. & Joshi, Y. C. 2015, *JApA*, 36, 33, <https://doi.org/10.1007/s12036-015-9327-z>
- Jurcsik, J., Sódor, Á., Váradi, M., et al. 2005, *A&A*, 430, 1049, <https://doi.org/10.1051/0004-6361:20041784>
- Leavitt, H. S. & Pickering, E. C. 1912, *HarCi*, 173, 1
- Lee, Y.-H., Kim, S. S., Shin, J., Lee, J., & Jin, H. 2008, *PASJ*, 60, 551, <https://doi.org/10.1093/pasj/60.3.551>
- Lenz, P. & Breger, M. 2005, *CoAst*, 146, 53, <https://doi.org/10.1553/cia146s53>
- Li, C. & Zhao, G. 2017, *ApJ*, 850, 25, <https://doi.org/10.3847/1538-4357/aa93f4>
- Lindegren, L., Lammers, U., Bastian, U., et al. 2016, *A&A*, 595, 4, <https://doi.org/10.1051/0004-6361/201628714>
- Luri, X., Brown, A. G. A., Sarro, L. M., et al. 2018, *A&A*, 616, 9, <https://doi.org/10.1051/0004-6361/201832964>
- McNamara, D. H. 2000, *ASPC*, 210, 373
- \_\_\_\_\_. 2011, *AJ*, 142, 110, <https://doi.org/10.1088/0004-6256/142/4/110>
- Mortara, L. & Fowler, A. 1981, *SPIE*, 290, 28, <https://doi.org/10.1117/12.965833>
- Niu, J.-S., Fu, J.-N., & Zong, W.-K. 2013, *RAA*, 13, 1181, <https://doi.org/10.1088/1674-4527/13/10/004>
- Niu, J.-S., Fu, J.-N., Li, Y., et al. 2017, *MNRAS*, 467, 3122, <https://doi.org/10.1093/mnras/stx125>
- Pamyatnykh, A. A. 1999, *AcA*, 49, 119
- Pecaut, M. J. & Mamajek, E. E. 2013, *ApJS*, 208, 9, <https://doi.org/10.1088/0067-0049/208/1/9>
- Pojmanski, G. 2000, *AcA*, 50, 177
- Poretti, E. 2003a, *A&A*, 409, 1031, <https://doi.org/10.1051/0004-6361:20031223>
- \_\_\_\_\_. 2003b, *ASPC*, 292, 145
- Qian, S.-B., Li, L.-J., He, J.-J., et al. 2018, *MNRAS*, 475, 478, <https://doi.org/10.1093/mnras/stx3185>
- Serenelli, A., Scott, P., Villante, F. L., et al. 2016, *MNRAS*, 463, 2, <https://doi.org/10.1093/mnras/stw1927>
- Shappee, B. J., Prieto, J. L., Grupe, D., et al. 2014, *ApJ*, 788, 48, <https://doi.org/10.1088/0004-637x/788/1/48>
- Smith, T. C., Henden, A. A., & Starkey, D. R. 2011, *SASS*, 30, 121
- Templeton, M. R., Samolyk, G., Dvorak, S., et al. 2009, *PASP*, 121, 1076, <https://doi.org/10.1086/630211>
- Vagnozzi, S., Freese, K., & Zurbuchen, T. H. 2017, *ApJ*, 839, 55, <https://doi.org/10.3847/1538-4357/aa6931>
- von Steiger, R. & Zurbuchen, T. H. 2016, *ApJ*, 816, 13, <https://doi.org/10.3847/0004-637x/816/1/13>
- Walker, G., Matthews, J., Kuschnig, R., et al. 2003, *PASP*, 115, 1023, <https://doi.org/10.1086/377358>
- Wang, R., Luo, A.-l., Zhang, S., et al. 2019, *PASP*, 131, 024505, <https://doi.org/10.1088/1538-3873/aaf25f>
- Warner, B. D. 2007, *MPBu*, 34, 113
- Wesselink, A. J. 1946, *BAN*, 10, 91
- Wils, P., Ayiomamitis, A., Robertson, C. W., et al. 2014, *IBVS*, 6122, 1
- Woźniak, P. R., Vestrand, W. T., Akerlof, C. W., et al. 2004, *AJ*, 127, 2436, <https://doi.org/10.1086/382719>
- Wunder, E. 2012, *BAVSR*, 61, 253
- Xiong, D. R., Deng, L., Zhang, C., & Wang, K. 2016, *MNRAS*, 457, 3163, <https://doi.org/10.1093/mnras/stw047>
- Zhao, G., Zhao, Y.-H., Chu, Y.-Q., Jing, Y.-P., & Deng, L.-C. 2012, *RAA*, 12, 723
- Ziaali, E., Bedding, T. R., Murphy, S. J., Van Reeth, T., & Hey, D. R. 2019, *MNRAS*, 486, 4348, <https://doi.org/10.1093/mnras/stz1110>